

SUPPLEMENTARY INFORMATION

NOVEL INHIBITOR DISCOVERY THROUGH VIRTUAL SCREENING AGAINST MULTIPLE PROTEIN CONFORMATIONS GENERATED VIA LIGAND-DIRECTED MODELING: A MATERNAL EMBRYONIC LEUCINE ZIPPER KINASE EXAMPLE

*Kiran V Mahasenan and Chenglong Li**

Division of Medicinal Chemistry and Pharmacognosy, College of Pharmacy, The Ohio State University,
Columbus, OH 43210.

CORRESPONDING AUTHOR: e-mail: li.728@osu.edu; phone: 614-247-8786

CONTENT

1. Table S1: MELK Inhibitor data collected from literature and their activity
2. Figure S1: MELK Inhibitor chemical structures
3. Table S2: Active compound dataset similarity/diversity matrix based on MACCS fingerprint Tanimoto coefficient.
4. Table S3: PDB Templates used in the modeling
5. Method details of MELK comparative modeling
6. Molecular dynamic simulation of MELK-inhibitor complex models
7. Figure S2: Plot of backbone RMSD (Y-axis) against snapshots written (X-axis) during MD simulation
8. Table S3: Decoy datasets used in the study
9. Figure S3: Alignment of all the MELK induced fit conformations based on binding site residues.
10. Figure S4: Binding site superposition of two underperformed MELK conformations.
11. Figure S5: Enrichment ROC plot for 5 decoy sets against all 22 MELK conformers
12. Figure S6: Enrichment ROC plot for 5 decoy sets against all 6 modeled apo MELK conformers
13. Table S4: Preliminary MELK kinase inhibition screening and kinome profiling
14. References

Table S1: MELK Inhibitor data collected from literature and their activity. (a¹, b² and c³)Activity is expressed as either Kd or percentage activity remained when tested at certain concentration. Availability of X-ray crystal data is also reported as yes (Y) or no (N)

Compound	Binding Assay		Single concentration Assay		Ref#	PDB
	Kd (nM)	%Activity remaining	Concentration tested			
Staurosporine	33				a	Y
VX-680	240	20	1	a,b	Y	
Sunitinib	350				a	Y
UCN-01		53	0.01	b	Y	
RO318220		61	0.1	b	Y	
A-443654		63	0.1	b	Y	
Purvalanol		72	0.1	b	Y	
Dorsomorphin		5	1	b	Y	
SP-600125		15	1	b	Y	
H89		43	1	b	Y	
Imatinib	1900				a	Y
Alsterpaullone		54	1	b	Y	
BX-320		57	1	b	Y	
PP2		57	1	b	Y	
PP1		58	1	b	Y	
C1	42			c	N	
PKC-412	280			a	N	
SU-14813	340			a	N	
AST-487	830			a	N	
GO-6976		15	0.1	b	N	
BX-795		32	0.1	b	N	
BI-D1870-R		40	0.1	b	N	
KT-5720		17	1	b	N	
CT-99021		45	1	b	N	
CHIR-258	1600			a	N	
BMS-387032	5600			a	N	
Kenpaullone		55	1	b	N	
CGP-57380		68	1	b	N	
SU-6668		73	1	b	N	

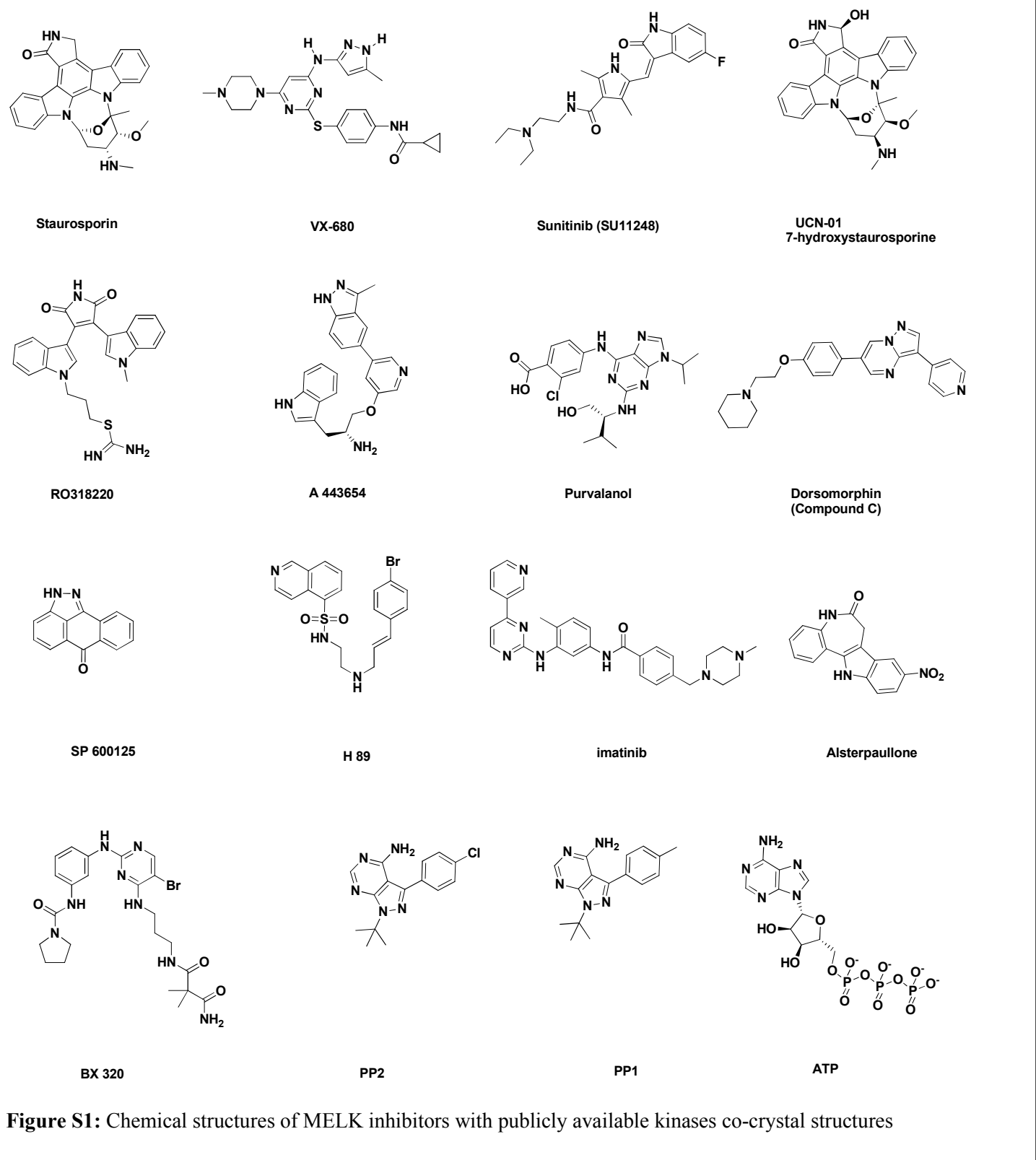


Figure S1: Chemical structures of MELK inhibitors with publicly available kinases co-crystal structures

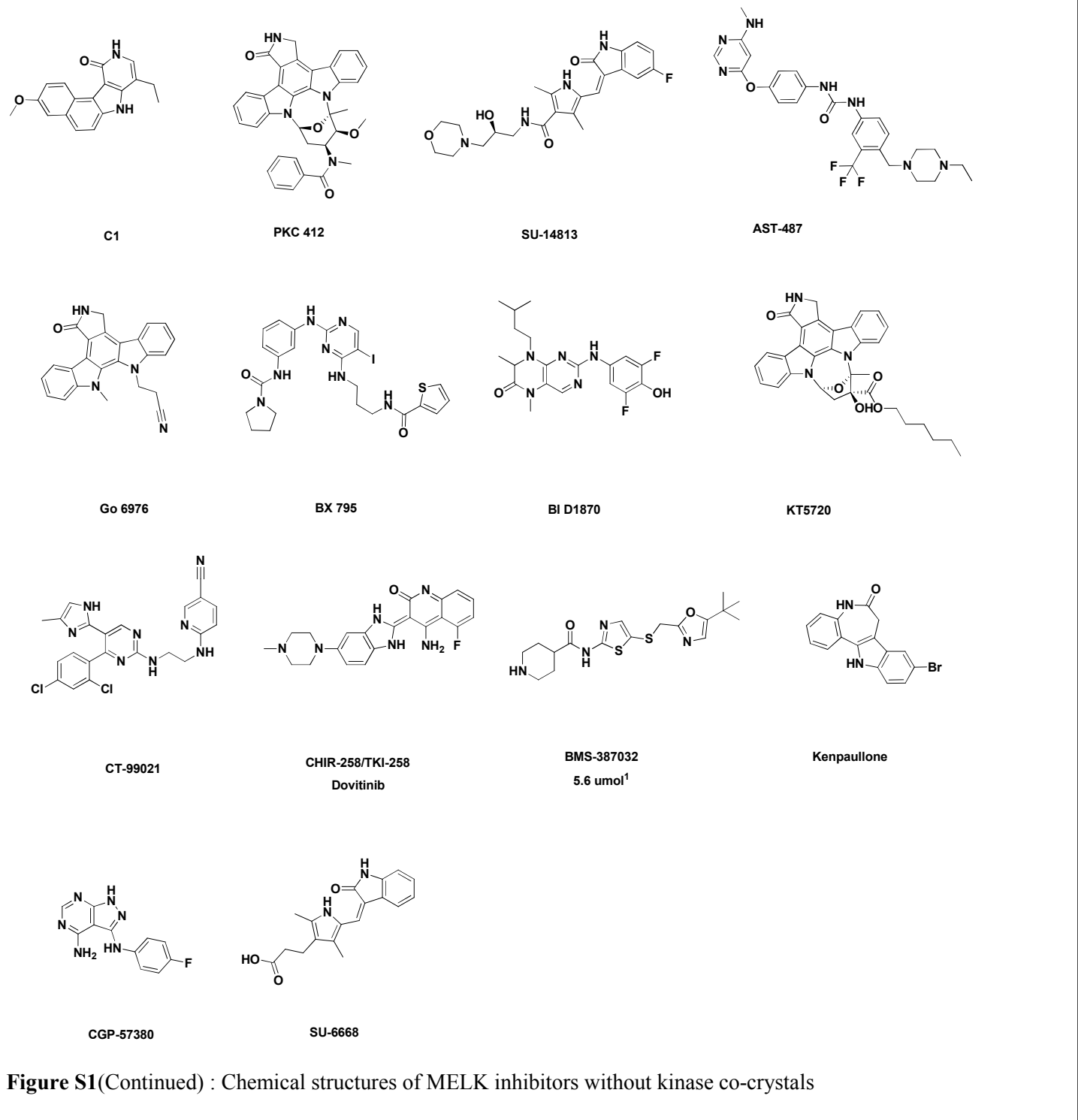


Figure S1(Continued) : Chemical structures of MELK inhibitors without kinase co-crystals

Table S2: Active compound dataset similarity/diversity matrix based on MACCS fingerprint Tanimoto coefficient.

Active compounds	01_Staurosporine	02_VX-680	03_Sunitinib	04_UCN-01	05_RO318220	06_A-443654	07_Purvalanol	08_Dorsomorphin	09_SP-600125	10_H89	11_Imatinib	12_Alsterpaullone	13_BX-320	14_ATP	15_PP1	16_ATP	17_C1	18_PKC-412	19_SU-14813	20_AST-487	21_GO-6976	22_BX-795	23_CT-99021	24_KT-5720	25_BI-D1870-R	26_CHIR-258	27_BMS-387032	28_Kenpaulone	29_CGP-57380	30_SU-6668	
01_Staurosporine	1.00	0.41	0.52	0.84	0.44	0.42	0.55	0.38	0.31	0.30	0.49	0.46	0.49	0.34	0.35	0.54	0.39	0.92	0.55	0.52	0.52	0.45	0.52	0.67	0.42	0.49	0.44	0.47	0.32	0.50	
02_VX-680	0.41	1.00	0.51	0.35	0.40	0.42	0.45	0.53	0.34	0.45	0.68	0.39	0.53	0.43	0.44	0.35	0.25	0.43	0.47	0.54	0.41	0.56	0.55	0.35	0.46	0.56	0.58	0.33	0.44	0.34	
03_Sunitinib	0.52	0.51	1.00	0.45	0.55	0.35	0.52	0.42	0.31	0.41	0.65	0.43	0.59	0.30	0.29	0.33	0.34	0.55	0.76	0.65	0.58	0.60	0.64	0.52	0.49	0.68	0.49	0.50	0.32	0.65	
04_UCN-01	0.84	0.35	0.45	1.00	0.38	0.39	0.52	0.35	0.32	0.22	0.42	0.45	0.42	0.33	0.34	0.51	0.41	0.84	0.49	0.49	0.45	0.38	0.46	0.64	0.36	0.42	0.35	0.49	0.31	0.49	
05_RO318220	0.44	0.40	0.55	0.38	1.00	0.38	0.39	0.34	0.33	0.36	0.43	0.41	0.41	0.29	0.30	0.34	0.40	0.39	0.49	0.38	0.62	0.41	0.43	0.40	0.37	0.55	0.45	0.42	0.26	0.62	
06_A-443654	0.42	0.42	0.35	0.39	0.38	1.00	0.45	0.61	0.54	0.34	0.32	0.45	0.31	0.48	0.50	0.47	0.51	0.40	0.41	0.32	0.37	0.33	0.35	0.34	0.38	0.31	0.34	0.40	0.49	0.38	
07_Purvalanol	0.55	0.45	0.52	0.52	0.39	0.45	1.00	0.38	0.30	0.32	0.57	0.43	0.59	0.45	0.42	0.52	0.36	0.52	0.55	0.50	0.46	0.61	0.62	0.48	0.64	0.49	0.49	0.47	0.41	0.50	
08_Dorsomorphin	0.38	0.53	0.42	0.35	0.34	0.61	0.38	1.00	0.37	0.35	0.44	0.33	0.42	0.42	0.44	0.44	0.35	0.42	0.52	0.47	0.40	0.44	0.44	0.43	0.38	0.44	0.35	0.30	0.40	0.32	
09_SP-600125	0.31	0.34	0.31	0.32	0.33	0.54	0.30	0.37	1.00	0.27	0.23	0.51	0.26	0.44	0.46	0.30	0.47	0.31	0.28	0.23	0.41	0.28	0.26	0.28	0.24	0.25	0.24	0.50	0.53	0.36	
10_H89	0.30	0.45	0.41	0.22	0.36	0.34	0.32	0.35	0.27	1.00	0.38	0.31	0.36	0.26	0.25	0.26	0.23	0.27	0.37	0.33	0.38	0.36	0.34	0.28	0.34	0.36	0.49	0.30	0.33	0.30	
11_Imatinib	0.49	0.68	0.65	0.42	0.43	0.32	0.57	0.44	0.23	0.38	1.00	0.37	0.67	0.31	0.32	0.36	0.28	0.52	0.59	0.70	0.51	0.72	0.76	0.43	0.60	0.65	0.56	0.38	0.28	0.44	
12_Alsterpaullone	0.46	0.39	0.43	0.45	0.41	0.45	0.43	0.33	0.51	0.31	0.37	1.00	0.38	0.37	0.39	0.38	0.35	0.43	0.39	0.34	0.43	0.43	0.40	0.33	0.36	0.40	0.39	0.68	0.43	0.48	
13_BX-320	0.49	0.53	0.59	0.42	0.41	0.31	0.59	0.42	0.26	0.36	0.67	0.38	1.00	0.42	0.41	0.36	0.29	0.52	0.56	0.69	0.48	0.81	0.69	0.43	0.62	0.57	0.64	0.46	0.36	0.44	
14_PP2	0.34	0.43	0.30	0.33	0.29	0.48	0.45	0.42	0.44	0.26	0.31	0.37	0.42	1.00	0.94	0.42	0.32	0.32	0.27	0.32	0.29	0.33	0.35	0.25	0.47	0.36	0.37	0.35	0.74	0.27	
15_PP1	0.35	0.44	0.29	0.34	0.30	0.50	0.42	0.44	0.46	0.25	0.32	0.39	0.41	0.94	1.00	0.44	0.33	0.33	0.26	0.31	0.31	0.32	0.34	0.26	0.43	0.35	0.38	0.33	0.73	0.28	
16_ATP	0.54	0.35	0.33	0.51	0.34	0.47	0.52	0.44	0.30	0.26	0.36	0.38	0.36	0.42	0.44	1.00	0.36	0.49	0.43	0.37	0.31	0.38	0.38	0.47	0.39	0.36	0.33	0.31	0.40	0.35	
21_C1	0.39	0.25	0.34	0.41	0.40	0.51	0.36	0.35	0.47	0.23	0.28	0.35	0.29	0.32	0.33	0.36	1.00	0.39	0.33	0.35	0.46	0.28	0.33	0.35	0.30	0.27	0.29	0.43	0.32	0.40	
22_PKC-412	0.92	0.43	0.55	0.84	0.39	0.40	0.52	0.42	0.31	0.27	0.52	0.43	0.52	0.52	0.32	0.33	0.49	0.39	1.00	0.57	0.57	0.52	0.48	0.54	0.67	0.42	0.49	0.40	0.47	0.30	0.47
23_SU-14813	0.55	0.47	0.76	0.49	0.49	0.41	0.55	0.52	0.28	0.37	0.59	0.39	0.56	0.27	0.26	0.43	0.33	0.57	1.00	0.54	0.60	0.56	0.57	0.44	0.62	0.47	0.45	0.29	0.58		
24_AST-487	0.52	0.54	0.65	0.49	0.38	0.32	0.50	0.47	0.23	0.33	0.70	0.34	0.69	0.32	0.31	0.37	0.35	0.57	0.54	1.00	0.46	0.66	0.79	0.48	0.52	0.62	0.49	0.39	0.32	0.43	
25_GO-6976	0.52	0.41	0.58	0.45	0.62	0.37	0.46	0.40	0.41	0.38	0.51	0.43	0.48	0.29	0.31	0.31	0.46	0.52	0.49	0.46	1.00	0.49	0.51	0.52	0.51	0.45	0.48	0.53	0.29	0.56	
26_BX-795	0.45	0.56	0.60	0.38	0.41	0.33	0.61	0.44	0.28	0.36	0.72	0.43	0.81	0.33	0.32	0.38	0.28	0.48	0.60	0.66	0.49	1.00	0.68	0.38	0.64	0.58	0.60	0.47	0.36	0.45	
27_BI-D1870-R	0.52	0.55	0.64	0.46	0.43	0.35	0.62	0.44	0.26	0.34	0.76	0.40	0.69	0.35	0.34	0.38	0.33	0.54	0.56	0.79	0.51	0.68	1.00	0.43	0.56	0.67	0.48	0.43	0.36	0.49	
28_KT-5720	0.67	0.35	0.52	0.64	0.40	0.34	0.48	0.43	0.28	0.43	0.33	0.43	0.45	0.25	0.26	0.47	0.35	0.67	0.57	0.48	0.52	0.38	0.43	1.00	0.36	0.39	0.37	0.21	0.50		
29_CT-99021	0.42	0.46	0.49	0.36	0.37	0.38	0.64	0.38	0.24	0.34	0.60	0.36	0.62	0.47	0.43	0.39	0.30	0.42	0.44	0.52	0.51	0.64	0.56	0.36	1.00	0.48	0.51	0.42	0.45	0.40	
31_CHIR-258	0.49	0.56	0.68	0.42	0.55	0.31	0.49	0.44	0.25	0.36	0.65	0.40	0.57	0.36	0.35	0.36	0.27	0.49	0.62	0.62	0.45	0.58	0.67	0.39	0.48	1.00	0.46	0.41	0.36	0.48	
32_BMS-387032	0.44	0.58	0.49	0.35	0.45	0.34	0.49	0.35	0.24	0.49	0.56	0.39	0.64	0.37	0.38	0.33	0.29	0.40	0.47	0.49	0.48	0.60	0.48	0.39	0.51	0.46	1.00	0.40	0.32	0.44	
33_Kenpaulone	0.47	0.33	0.50	0.49	0.42	0.40	0.47	0.30	0.50	0.30	0.38	0.68	0.46	0.35	0.33	0.31	0.43	0.47	0.45	0.39	0.53	0.47	0.43	0.37	0.42	0.41	0.40	1.00	0.41	0.54	
34_CGP-57380	0.32	0.44	0.32	0.31	0.26	0.49	0.41	0.40	0.53	0.33	0.28	0.43	0.36	0.74	0.73	0.40	0.32	0.30	0.29	0.32	0.29	0.36	0.21	0.45	0.36	0.32	0.41	1.00	0.29		
35_SU-6668	0.50	0.34	0.65	0.49	0.62	0.38	0.50	0.32	0.36	0.30	0.44	0.48	0.44	0.27	0.28	0.35	0.40	0.47	0.58	0.43	0.56	0.45	0.49	0.50	0.40	0.48	0.44	0.54	0.29	1.00	

Table S3: PDB Templates used in the modeling

Model#	Model ID	Inhibitor	hMEK potency/affinity	Conf. State	Strt #	#	PDB	Protein	Crystal Complex ligand	Ligand ID	Res. (Å)	Organism	Sequence Analysis with BLAST				
													Identity	Similarity	Alignment	Gaps	Bit Score
1	STU	Staurosporine	33 nM	Active	1	1	1NVR	Cdk1	Staurosporin	STU	1.80	Human	34	54	256	4	157
					2	2	1STC	PKA	Staurosporin	STU	1.80	Human	38	53	262	14	158
					3	3	1WWY	DAP kinase	Staurosporin	STU	2.30	Human	33	54	266	16	150
					4	4	1OKY	PDK1	Staurosporin	STU	2.30	Human	31	53	251	6	139
					5	5	2ZTR	RSK1	Staurosporin	STU	2.00	Human	31	56	248	10	139
					6	6	1NWK	MAP KAP kinase-2	Staurosporin	STU	2.70	Human	31	53	259	32	126
					7	7	1XUD	PKC-theta	Staurosporin	STU	2.80	Human	30	50	253	6	123
2	VX6	VX-680	240 nM	Active	1	8	3E5A	Aurora A Ab1	VX-680	VX6	2.30	Human	30	55	255	6	152
					2	9	2F4J		VX-680	VX6	1.91	Human	23	45	247	11	74
3	B49	Sunitinib	650 nM	Inactive	1	10	2J4M	CAMK1G	SU-11652	J60	1.70	Human	35	59	256	12	174
					2	11	3HZT	CDPK3	SU-11652	J60	2.00	Toxoplasma	37	57	263	15	169
					3	12	2J4V	NEK2	S25	S25	2.20	Human	29	49	266	15	100
					4	13	3MIY	TK	Sunitinib (SU-11248)	B49	1.67	Human	27	46	252	13	77
					5	14	3GCE	KT	Sunitinib (SU-11248)	B49	1.60	Human	24	43	272	29	63
					6	15	3GCF	KT (Mutant)	Sunitinib (SU-11248)	B49	2.60	Human	24	43	272	29	63
4	UCN	UCN-01	53% (0.01)	Active	1	16	1NQJ	Cdk1	UCN-01	UCN	2.00	Human	35	55	256	4	157
					2	17	1OKZ	PDK1	UCN-01	UCN	2.51	Human	32	54	251	6	132
					3	18	1PKD	CDK2	UCN-01	UCN	2.30	Human	31	45	282	36	107
5	DRN	R-0318220	61% (0.1 μM)	Active	1	19	2V70	CANK2q	RO318220	DRN	2.25	Human	33	55	261	6	152
					2	20	2U2U	PKA-a	A443654	L20	2.40	Bovine	35	53	261	5	158
6	I20	A-443654	63% (0.1 μM)	Active	2	21	2JDV	PKA-a (mut)	A443654	L20	2.08	Bovine	36	53	261	6	155
					3	22	2JDS	PKA-a	A443654	L20	2.00	Bovine	35	53	261	6	152
					4	23	2JDR	RAC-beta/Alt-2	A443654	L20	2.30	Human	35	56	239	3	150
					1	24	1CKP	CDK2	PURVALANOL B	PVB	2.05	Human	31	45	262	36	107
7	PVB	PVB	72% (0.1 μM)	Inactive	2	25	1V0P	PRK5	PURVALANOL B	PVB	2.00	P. falciparum	29	47	287	37	94
					3	26	2X7G	SRPK2	PURVALANOL B	PVB	2.50	Human	28	47	75	3	31
					1	27	3H9R	ACVR1	Dorsomorphin	TAK	2.35	Human	26	44	213	10	50
8	TAK	Dorsomorphin	5% (1 μM)	Active	1	28	27MD	MSP1	SP600125	537	2.88	Human	29	47	274	10	85
					2	29	1PMV	JNK3	SP600125	537	2.50	Human	26	43	303	11	74
					3	30	1UKI	JNK1	SP600125	537	2.70	Human	26	42	302	10	71
10	IQB	H89	43% (1 μM)	Active	1	31	1YDT	PKA	H89	QB	2.30	Cattle	34	52	261	5	150
					2	32	3GVU	Ab12	Imatinib	STI	2.05	Human	26	47	244	11	88
					3	33	3HEC	p38	Imatinib	STI	2.50	Human	25	44	291	44	86
					4	34	20IQ	c-Src	Imatinib	STI	2.07	Human	30	46	250	11	84
					5	35	2PLD	LOK	Imatinib	STI	2.80	Human	27	49	217	10	82
					6	36	3KEV	Ab11	Imatinib	STI	1.74	Human	23	45	247	11	77
					7	37	1IEP	Ab11	Imatinib	STI	2.10	Human	23	45	247	11	75
					8	38	1OPJ	Ab11	Imatinib	STI	1.75	Human	23	45	247	11	75
					9	39	2HYY	Ab11	Imatinib	STI	2.40	Human	23	45	247	11	75
					10	40	1XEB	SYK	Imatinib	STI	1.57	Human	24	46	190	9	63
12	ATU	Aisterpaulone	54% (1 μM)	Active	1	42	1Q3W	GSK-3beta	Aisterpaulone	ATU	2.30	Human	34	50	218	27	79
					2	43	1Z5M	PDK1	BX 320	L18	2.17	Human	31	53	261	4	138
14	PP2	PP2	57% (1 μM)	Active	1	44	3GEQ	SIC	FP2	PP2	2.20	Chicken	30	46	250	8	82
					2	45	1OFP	I1K	FP2	PP2	2.00	Human	27	50	217	7	82
					3	46	2ZV9	Lyn	FP2	PP2	2.76	Mouse	26	48	227	18	78
15	PP1	PP1	50% (1 μM)	Active	1	47	1QCF	HCK	FP1	PP1	2.00	Human	26	50	222	7	80
					2	48	2MV	RET	FP1	PP1	2.25	Human	25	43	272	9	69
16	ATP	ATP	50 μM	Active	1	49	1CDK	PKA	ANP	ATP	2.00	Pig	35	53	261	5	156
					2	50	1Q24	PKA	ATP	ATP	2.60	Cattle	35	53	281	6	154
					3	51	1ATP	PKA	ATP	ATP	2.20	Mouse	35	53	257	6	149
					4	52	1LR3	PKA	ADP	ADP	2.00	Mouse	35	52	257	6	145
					5	53	1R0U	PKA	ATP	ATP	1.26	Mouse	35	52	257	6	144
					6	54	1QL6	PKA	ATP	ATP	2.40	Rabbit	34	52	272	8	143
					7	55	2BIY	PDK1	ATP	ATP	1.95	Human	31	53	251	4	139

Method details of MELK comparative modeling

Since there was wide sequence identity range for MELK templates among different chemotypes, preliminary models of the MELK showed varied overall protein fold. This was especially noticeable at the C-terminus lobe of the models away from the catalytic residues. These variable structural folds play more of a regulatory role than a direct role in the catalytic reaction and hence the structural dissimilarity among the templates. As the sequence identity to templates dropped below 30%, the models became more deviated from the general population of ensemble. For example, C-terminus folds of modeled PP1 were different from PP2, although the inhibitor chemical structures were quite similar. The two templates with co-crystallized PP1 had only 26% (HCK) and 25% (RET) sequence identity to MELK. While it is possible for the enzyme to undergo large shift in the overall fold on ligand binding, a superposition of the same protein kinase X-ray crystal structures bound to different inhibitors shows that major conformational change upon ligand binding occur at the N-lobe whereas the C-terminus kinase domain remains largely unaffected by ATP site directed ligands. This is observable when several PKA crystal structures (1STC, 2UZU, 1YDT, 1CDK) or PDK1 crystal structures (1OKY, 1OKZ, 2BIY) bound to different ATP directed ligands are superimposed. We selected Staurosporine bound form as the study system for the initial fold modeling validation. A molecular dynamic study of Staurosporine bound A-loop phosphorylated MELK model proved the stability of the overall fold revealing the critical residues in the protein stability. Hence, when the model deviated from this MELK-Staurosporine overall C-terminus fold, manual alignment was performed by utilization of the co-ordinate from closer homologues or successful MELK models from other chemotype templates. At the same time, we ensured that the binding site shape for the specific chemotype was not drastically altered in the modeling process. This C-terminal modeling of the secondary structures far away from binding site may not significantly affect the molecular docking studies since we only consider the residues in the binding pocket for the calculation. However, our effort was to model the MLEK conformation as close to its biological state as possible to study the enzyme as a functional unit and to probe any potential druggable allosteric binding sites.

Molecular dynamic simulation of MELK-inhibitor complex models:

The models were subjected to minimization and NPT molecular dynamics simulation for 5 ns duration with Desmond v2.2. TIP3P water model with an orthorhombic box of 10Å buffer was used in the setup stage neutralizing the whole system with charge-balancing counter ions. To simulate the ionic salt concentration as in the experimental condition, 0.025 M NaCl was added to the system. Default parameters were applied to the simulation, which uses OPLS 2005 force field recording energy at 1.2 ps intervals and writing out trajectory at 4.8 ps intervals.

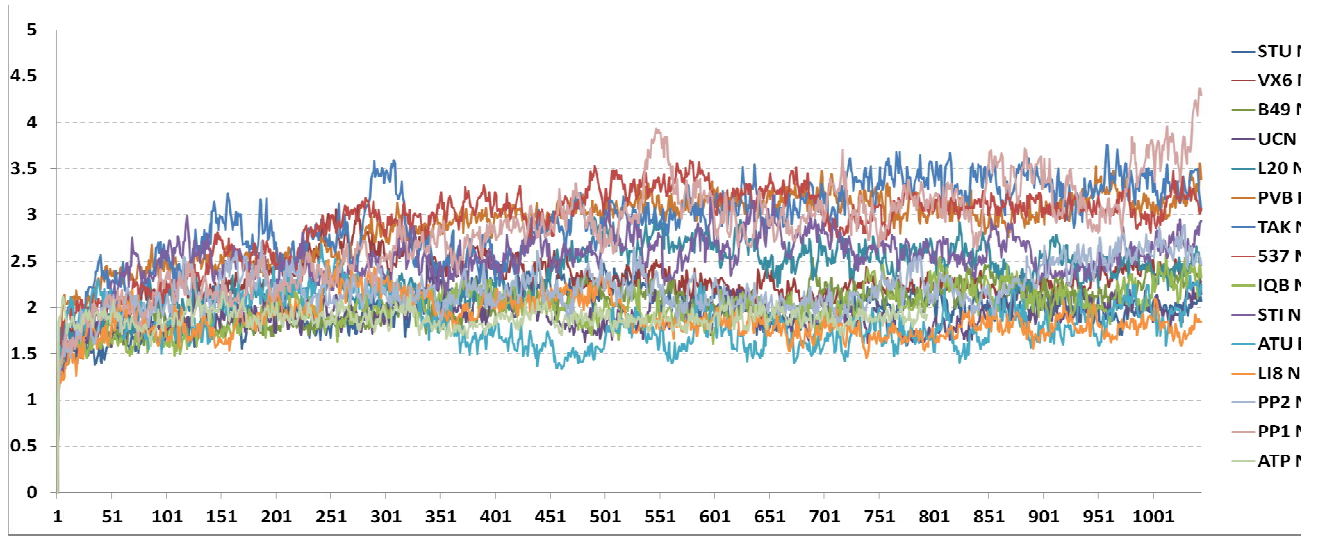


Figure S2: Backbone RMSD (Y-axis, in Å) against number of snapshots written (X-axis) each at 4.8ps interval of 5 ns molecular dynamic simulations of MELK ligand bound conformations. A relatively stable trajectory was obtained in the process.



Figure S3: Alignment of all the MELK induced fit conformations based on binding site residues. Hydrogen bonds formed by the inhibitors to the MELK hinge residues are highlighted as yellow dashed lines.

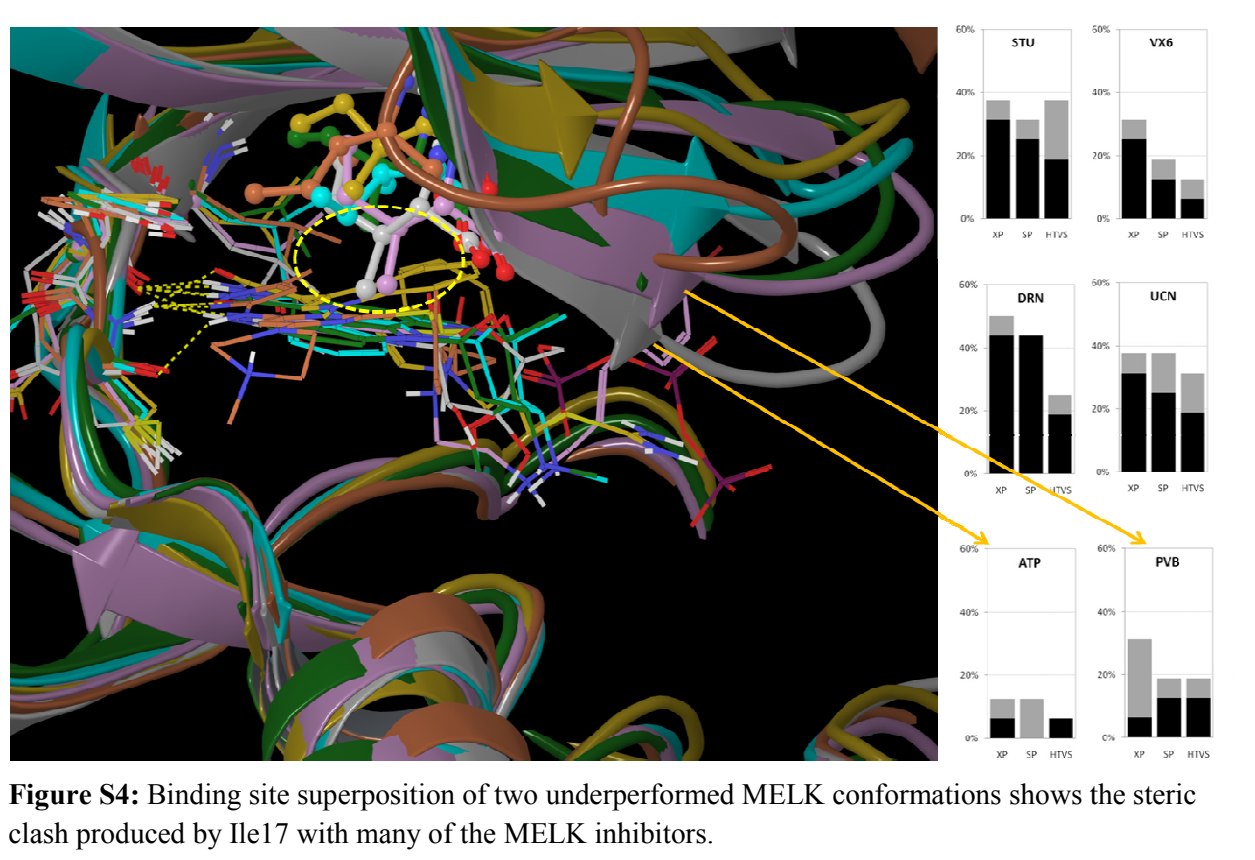


Table S3: Decoy datasets used in the study

Decoy set	No of compounds	Description	Reference
SCH	1000	Pooled from chemical collections of pharmaceutical corporate databases. Averaged molecular weight of 400. This collection has already been studied for evaluation of Glide program by the developers.	⁴
CMN	1000	Randomly selected 1000 molecules from MDL Drug Data Report (MDDR).	⁵
ROG	861	The original dataset consist of 990 nonreactive organic molecules randomly chosen from the Advanced Chemical Directory (ACD). Later Jain et al refined the dataset by removing ligands with greater than 15 rotatable bonds.	^{6, 7}
JAI	1000	Randomly selected from druglike ZINC database subset	⁷
DUD	1779	The kinase specific CDK2 decoy subset of DUD	⁸

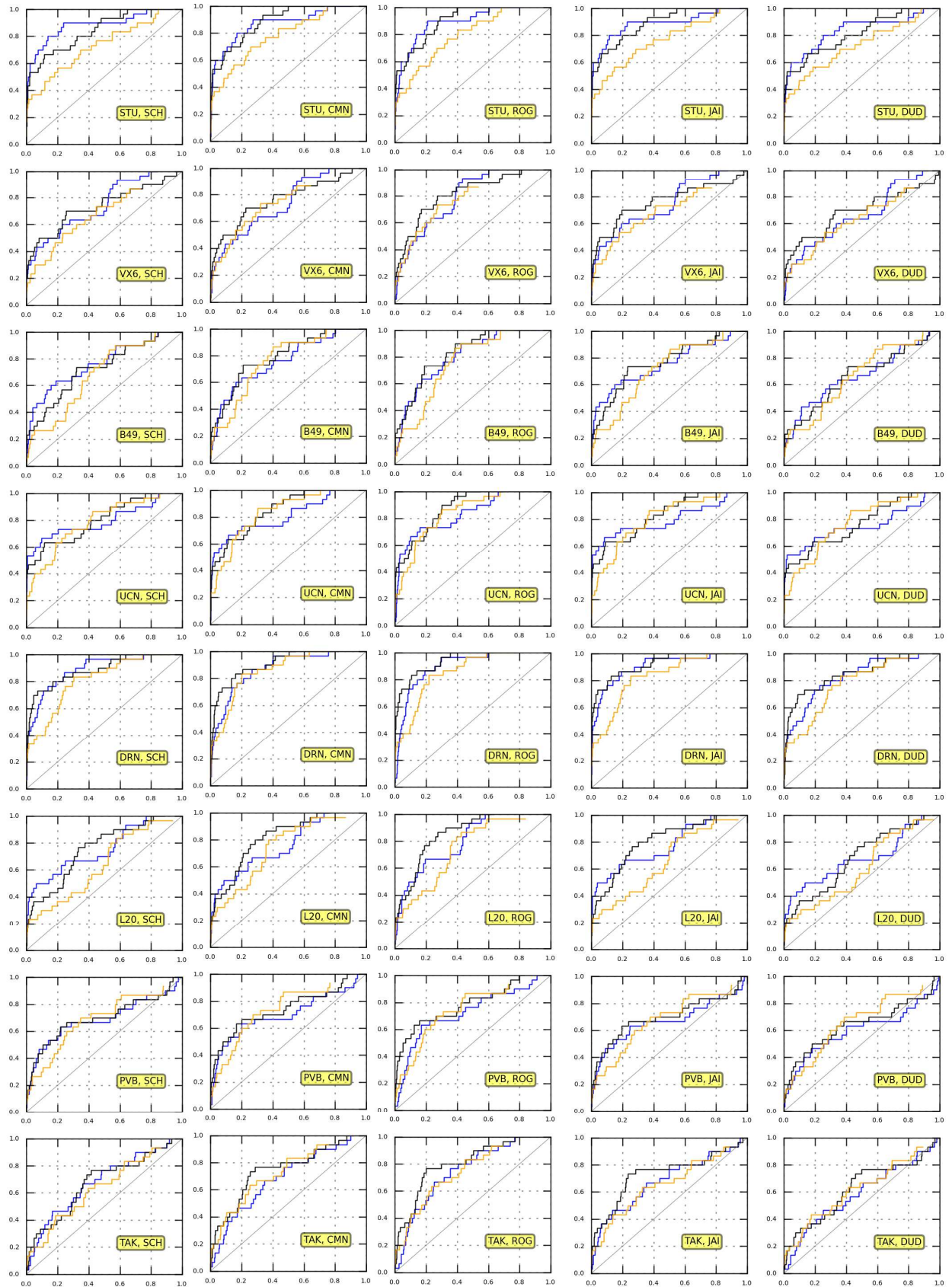


Figure S5: Enrichment ROC plot for 5 decoy sets against the induced fit MELK conformers. (Glide XP=Blue, SP=Black and HTVS=Orange). First 3 letter code corresponds to the MELK conformer while the second one correspond to the decoy set used. Each row comprise to a particular conformer and each column corresponds to a decoy data set.

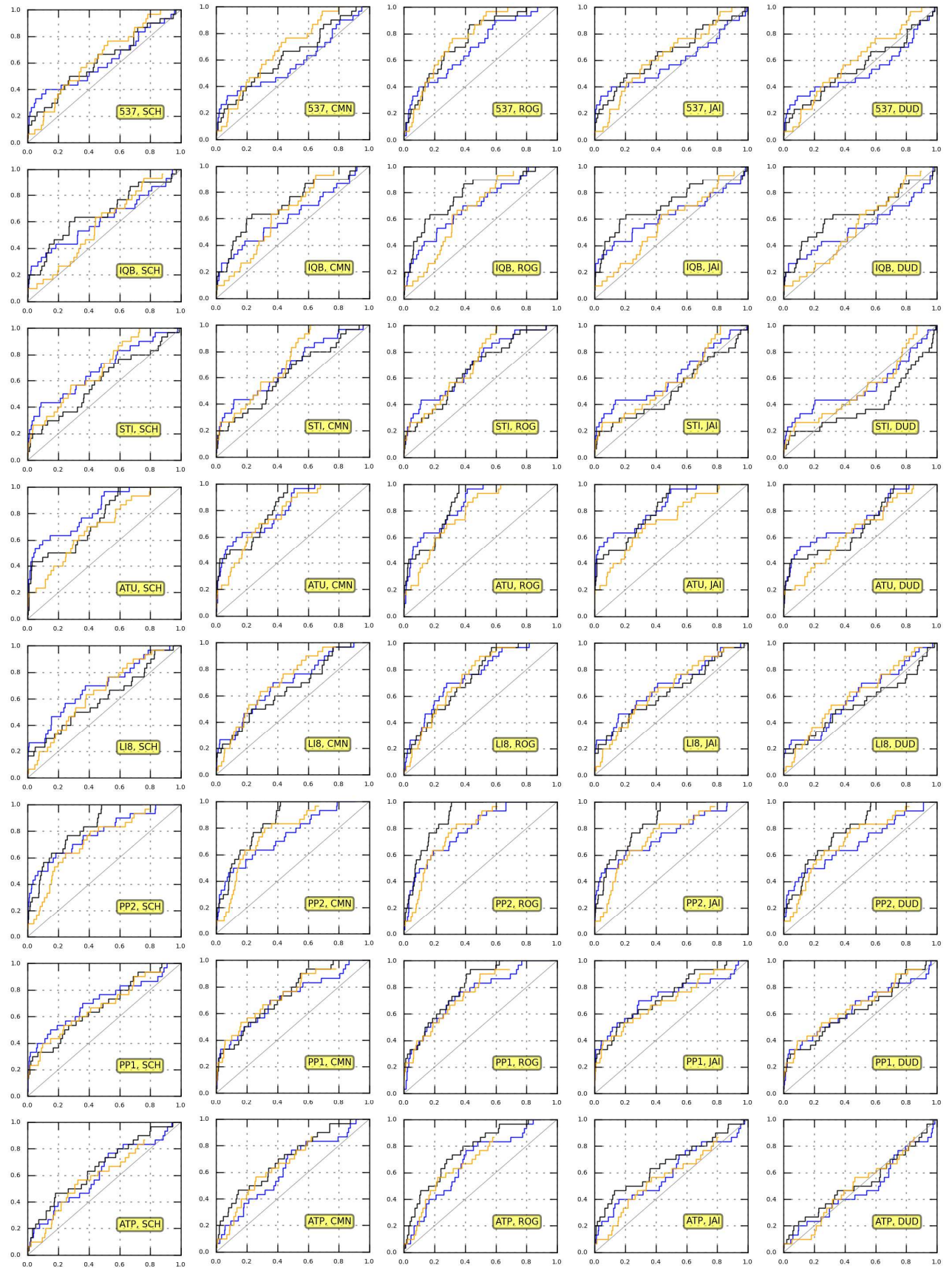


Figure S5 (continued..)

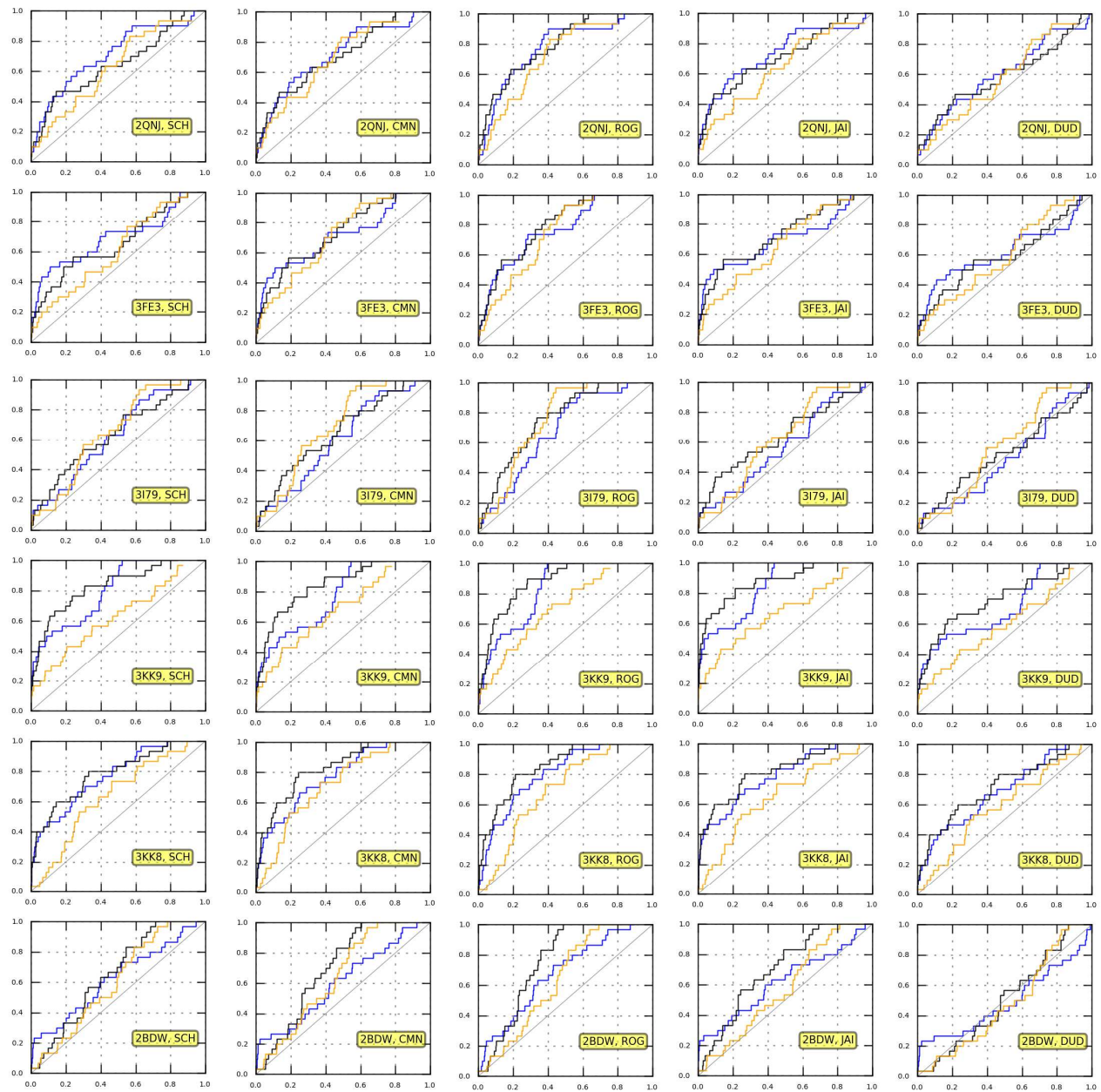


Figure S6: Enrichment ROC plot for 5 decoy sets against all 6 modeled unliganded MELK conformers. (Glide XP=Blue, SP=Black and HTVS=Orange). First 4 letter code for each ROC plot corresponds to the unliganded MELK conformer while the second code correspond to the decoy set used. Each row comprise to a particular conformer and each column corresponds to a decoy data set used in the screening.

Table S4: Preliminary MELK kinase inhibition screening and kinome profiling of *in silico* hits selected through ensemble virtual screen.

Compound ID	MELK	AMPK-alpha2	AURKA	CAMK2G	PKAC-alpha	ChemBridge ID
1	93	100	92	96	95	5378519
2	88	97	99	98	100	5646884
3	100	91	89	100	100	6048495
4	96	88	91	91	100	6238977
5	98	100	100	94	100	6336332
6	88	86	75	93	100	6617586
7	88	100	80	86	100	6643218
8	100	91	91	92	100	7034472
9	52	98	99	90	100	7092361
10	100	94	99	100	100	7330793
11	100	88	100	100	100	7417888
12	66	97	90	86	100	7650649
13	92	97	93	100	100	7802635
14	79	97	92	84	100	7912202
15	27	100	72	77	100	7932356
16	65	83	87	83	100	7963735
17	86	94	84	99	100	9007867
18	100	93	100	100	100	9019583
19	91	100	100	90	100	9108235
20	73	81	99	99	100	9125772
21	99	100	90	96	100	9195764
22	97	98	95	95	97	9199018
23	95	68	86	97	94	9252630

REFERENCES

1. Karaman, M. W.; Herrgard, S.; Treiber, D. K.; Gallant, P.; Atteridge, C. E.; Campbell, B. T.; Chan, K. W.; Ciceri, P.; Davis, M. I.; Edeen, P. T.; Faraoni, R.; Floyd, M.; Hunt, J. P.; Lockhart, D. J.; Milanov, Z. V.; Morrison, M. J.; Pallares, G.; Patel, H. K.; Pritchard, S.; Wodicka, L. M.; Zarrinkar, P. P. A quantitative analysis of kinase inhibitor selectivity. *Nat Biotechnol* **2008**, 26, 127-32.
2. Bain, J.; Plater, L.; Elliott, M.; Shpiro, N.; Hastie, C. J.; McLauchlan, H.; Klevernic, I.; Arthur, J. S.; Alessi, D. R.; Cohen, P. The selectivity of protein kinase inhibitors: a further update. *Biochem J* **2007**, 408, 297-315.
3. Hoang, T. M.; Favier, B.; Valette, A.; Barette, C.; Nguyen, C. H.; Lafanechere, L.; Grierson, D. S.; Dimitrov, S.; Molla, A. Benzo[e]pyridoindoles, novel inhibitors of the aurora kinases. *Cell Cycle* **2009**, 8, 765-72.
4. Friesner, R. A.; Banks, J. L.; Murphy, R. B.; Halgren, T. A.; Klicic, J. J.; Mainz, D. T.; Repasky, M. P.; Knoll, E. H.; Shelley, M.; Perry, J. K.; Shaw, D. E.; Francis, P.; Shenkin, P. S. Glide: a new approach for rapid, accurate docking and scoring. 1. Method and assessment of docking accuracy. *J Med Chem* **2004**, 47, 1739-49.
5. Cummings, M. D.; DesJarlais, R. L.; Gibbs, A. C.; Mohan, V.; Jaeger, E. P. Comparison of automated docking programs as virtual screening tools. *J Med Chem* **2005**, 48, 962-76.
6. Bissantz, C.; Folkers, G.; Rognan, D. Protein-based virtual screening of chemical databases. 1. Evaluation of different docking/scoring combinations. *J Med Chem* **2000**, 43, 4759-67.
7. Pham, T. A.; Jain, A. N. Parameter estimation for scoring protein-ligand interactions using negative training data. *J Med Chem* **2006**, 49, 5856-68.
8. Huang, N.; Shoichet, B. K.; Irwin, J. J. Benchmarking sets for molecular docking. *J Med Chem* **2006**, 49, 6789-801.